XL CILAMCE
IBERO-LATIN AMERICAN CONGRESS ON COMPUTATIONAL METHODS IN ENGINEERING
NOVEMBER 11-14, 2019
Praiamar Natal Hotel & Convention Natal, RN-BRAZIL

NUMERICAL MODELING OF REINFORCED CONCRETE BEAMS USING THE COMPOSITION OF TWO PLASTIFICATION SURFACES

Matheus E. Benincá
Inácio B. Morsch
matheuseb@hotmail.com
morsch@ufrgs.br
Programa de Pós-Graduação em Engenharia Civil - UFRGS
Av. Osvaldo Aranha, 99, 90035-190, Porto Alegre, RS, Brasil

Abstract. In order to consider the multiaxial behavior of concrete, several plastification and rupture surfaces have already been proposed, such as the Ottosen surface or the Willam-Warnke surface. However, the use of these surfaces in numerical finite element models can often lead to convergence difficulties, due to the complexity of their formulations. In this context, the present work simulated numerically the behavior of two reinforced concrete beams tested experimentally in a previous work, using ANSYS software, version 19.2, with a new elastoplastic model available in the recent versions of this software, denominated DP-Concrete. This model uses the composition of two simpler plastification surfaces, one for tensile behavior, which can be a Rankine or a Drucker-Prager surface, and another Drucker-Prager surface for compressive behavior. This surface composition allows simulating the large differences in the concrete behavior under tension and compression, which would not be possible with a single Drucker-Prager surface. In addition, because it is a newly available material model, it can be applied to the SOLID186 element, which is classified as a current-technology element by this software, and therefore is compatible with several current ANSYS features, such as the generation of embedded elements by the mesh-independent method, through the MESH200 guide elements, which were also used in this work. In order to consider the cracking and crushing phenomena, different softening and hardening laws available in the software were used. The obtained results were compared with each other and with the results of the experimental tests. In addition, numerical analyses were performed with a customized material model based on the Ottosen criterion, whose results were also used for comparison purposes. It was concluded that the DP-Concrete model is an adequate modeling strategy for the concrete behavior, and its main advantages are its simplicity, flexibility and compatibility with other current ANSYS functionalities.

Keywords: Finite Element Method, Concrete, Drucker-Prager, Rankine, Surfaces Composition.

1 Introduction

The numerical simulation of reinforced concrete structures can become quite complex, due to large differences in tensile and compressive behavior of concrete, as well by the cracking and crushing phenomena. In order to achieve these objectives, finite element programs often implement different plastification surfaces and constitutive models. Chen [1] presents models that can be adjusted to the plastification and rupture surfaces of the concrete, from 1 parameter models (e.g. Rankine), 2 parameters (e.g. Drucker and Prager [2]), 3 parameters (e.g. Willam and Warnke [3]), 4 parameters (e.g. Ottosen [4]) and 5 parameters (e.g. modified Willam-Warnke). Although a model with a larger number of parameters can theoretically represent more accurately the actual behavior of the concrete, it is necessary to consider that increasing the number of parameters also increases the surface shape complexity, therefore more convergence problems may appear. For example, Queiroz et al. [5] cited convergence problems while using the Willam-Warnke model, which had been implemented in previous versions of ANSYS. In addition, the utilization of this model is no longer recommended in version 19.2 of ANSYS, used in the present work, because it is only compatible with the hexahedral finite element SOLID65, which is classified as a legacy-element by the software manual [6]. The Ottosen model [4], on the other hand, was implemented by Lazzari et al. [7] in ANSYS through the usermat interface, which allows the customization of a material model, but is not available in the commercial versions of the software.

In this context, an alternative is the utilization of a new model composed by two different uncomplicated surfaces, one for tensile behavior (Rankine or Drucker-Prager), and another for compressive behavior (Drucker-Prager). In ANSYS, this model is called DP-Concrete, and has been made available in its most recent versions. For the simulation of crushing and cracking, different hardening and softening rules are provided by the software.

The present work aims to evaluate this new model in the simulation of two reinforced concrete beams tested experimentally by Bresler and Scordelis [8]. In addition, analyses will be performed with the customized model based on the surface of Ottosen [4].

2 Numerical model

In this section, the numerical model developed in ANSYS is presented, showing the element types, the material models and the boundary conditions used.

2.1 Element types

The concrete beam was modeled by hexahedral elements with twenty nodes and three degrees of freedom per node (translations in x, y and z), called SOLID186 in ANSYS [6]. In the present work these elements were used in their homogeneous form with full integration. Its formulation is based on Zienkiewicz [9]. Because it is a current-technology element, SOLID186 is compatible with several current ANSYS features, such as the generation of embedded elements and the use of new material models, e.g. DP-Concrete.

The reinforcement bars were modeled by discrete embedded elements, called REINF264 in ANSYS [6], which are suitable for simulating steel bars. These elements use the same nodes of the base elements SOLID186, even if their geometric position does not coincide with them. The REINF264 element presents only axial stiffness, thus the stiffnesses to bending, torsion and shear stress are neglected. A perfect interaction between the reinforcing element and the concrete base element is admitted, so there is no relative movement between them [6].

For the generation of reinforcement embedded elements, a new ANSYS functionality was used, which is denominated mesh-independent method. This method uses MESH200 elements, which are only guide elements, and thus do not directly contribute to the solution, but determine the positions where REINF264 reinforcement elements are created. Therefore, it is possible to insert the positions of the reinforcement bars from the lines drawn in absolute coordinates, unlike the standard method, in which it is necessary to use relative coordinates in respect to the base elements, which generates mesh

dependence. Figure 1 illustrates the elements SOLID186 (in black) and REINF264 (in red).

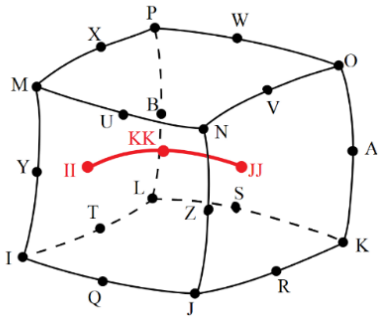

Figure 1. Elements SOLID186 and REINF264 [6].

2.2 Material models

This section presents the material models used for concrete and steel. In the case of concrete, two models are presented: (i) DP-Concrete and (ii) customized model via ANSYS usermat interface.

2.2.1 DP-Concrete

A single Drucker-Prager surface does not represent the large differences in tensile and compressive behavior of concrete. Thus, the DP-Concrete model uses a Drucker-Prager plastification surface for compression, and a second surface, which may be Drucker-Prager or Rankine, for tension and tension-compression. Figure 2 illustrates the two possible compositions (referred to as DP-DP or DP-Rankine) in the two-dimensional principal stress plane. The surfaces formulations are presented below, based on Chen [1] and ANSYS [6].

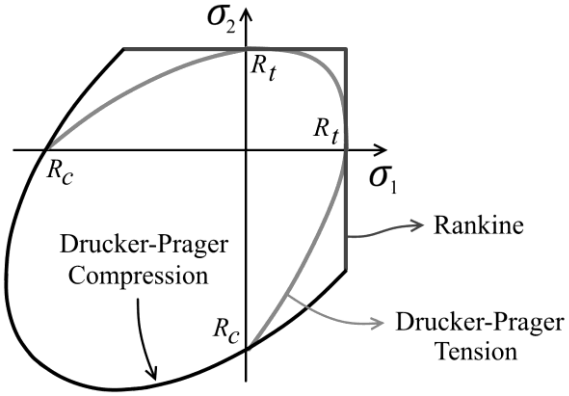

Figure 2. Combinations DP-DP or DP-Rankine (adapted from [6]).

The Drucker-Prager surface in tension and tension-compression is defined by Eq. (1).

$$f_{DPt} = \frac{\sigma_e}{\sqrt{3}} + \beta_t . \sigma_m - \sigma_{Yt} = 0. \tag{1}$$

Where $\sigma_m = I_1/3$ is the hydrostatic stress; I_1 is the first stress invariant; J_2 is the second deviatoric stress invariant; $\sigma_e = \sqrt{3J_2}$ is the von Mises stress; and β_t, σ_{Yt} are values calculated from material parameters and HSD model functions.

While the value of f_{DPt} is less than zero, the behavior in tension and tension-compression is admitted as linear elastic. When f_{DPt} equals zero, the plastic regime is started, in which the cracking phenomenon can be simulated, approximately, by increments of plastic strain. In this step, the values of β_t and σ_{Yt}, both constant in the elastic regime, can vary according to the functions Ω_c and Ω_t, which, in

turn, depend on the adopted HSD model. This variation determines how the plastification surface moves in the plastic regime. The Eq. (2) and (3) define the values of β_t and σ_{Yt}.

$$\beta_t = \frac{\sqrt{3}.(R_c.\Omega_c - R_t.\Omega_t)}{R_c.\Omega_c + R_t.\Omega_t}. \tag{2}$$

$$\sigma_{Yt} = \frac{2.R_c.\Omega_c.R_t.\Omega_t}{\sqrt{3}.(R_c.\Omega_c + R_t.\Omega_t)}. \tag{3}$$

Where R_c is the uniaxial compressive strength of concrete [kN/cm²]; R_t is the uniaxial tensile strength of concrete [kN/cm²]; Ω_c is the compression function of the adopted HSD model (dimensionless); Ω_t is the tension function of the adopted HSD model (dimensionless).

The Rankine surface in tension and tension-compression is defined by Eq. (4).

$$f_R = \sigma_m + \frac{2}{3}.\sigma_e.cos(\theta) - T.\Omega_t = 0. \tag{4}$$

$$\cos(3\theta) = \frac{3\sqrt{3}}{2}.\frac{J_3}{\sqrt{J_2^3}}. \tag{5}$$

Where θ is the similarity angle, defined by Eq. (5); J_3 is the third deviatoric stress invariant; T is the uniaxial tensile strength of concrete.

While the value of f_R is less than zero, the tensile and tensile-compressive behavior is admitted as linear elastic. When f_R equals zero, the plastic regime starts, in which the cracking can be simulated, approximately, through increments of plastic strain. In this step, the Rankine surface moves according to the function Ω_t of the adopted HSD model.

The Drucker-Prager surface under compression is defined by Eq. (6).

$$f_{DPc} = \frac{\sigma_e}{\sqrt{3}} + \beta_c.\sigma_m - \sigma_{Yc}.\Omega_c = 0. \tag{6}$$

Where β_c, σ_{Yc} are the constants calculated from material parameters.

While the value of f_{DPc} is less than zero, the behavior in compression is admitted as linear elastic. When f_{DPc}equals zero, the plastic regime starts: the Drucker Prager surface moves according to the function Ω_c of the adopted HSD model. As a general rule, unless concrete is accepted as perfectly elastoplastic (without the adoption of any HSD model), all available HSD models are divided into two sections in the compression behavior: (i) hardening, which governs surface expansion, until the maximum compressive stress is reached; and (ii) softening, which governs the shrinkage of the surface, initiating the crushing process, after reaching the maximum compressive stress.

The values of the constants β_c e σ_{Yc} are calculated by Eq. (7) and (8).

$$\beta_c = \frac{\sqrt{3}.(R_b - R_c)}{2.R_b - R_c}. \tag{7}$$

$$\sigma_{Yc} = \frac{R_b.R_c}{\sqrt{3}.(2.R_b - R_c)}. \tag{8}$$

Where R_b is the biaxial compressive strength of concrete [kN/cm²].

Depending on the HSD (hardening, softening and dilatation) model adopted, the functions Ω_c and Ω_t assume a certain format. Through these models, it is possible to simulate, approximately, the

phenomena of cracking, in the tensile behavior, and crushing, in the compressive behavior, through increments of plastic strain related to hardening and softening rules. ANSYS offers four types of HSD models. In this work, three of them (Linear, Exponential and Steel Reinforcement) were used, shown in Fig. 3. If no HSD model is adopted, the software admits the material as perfectly elastoplastic.

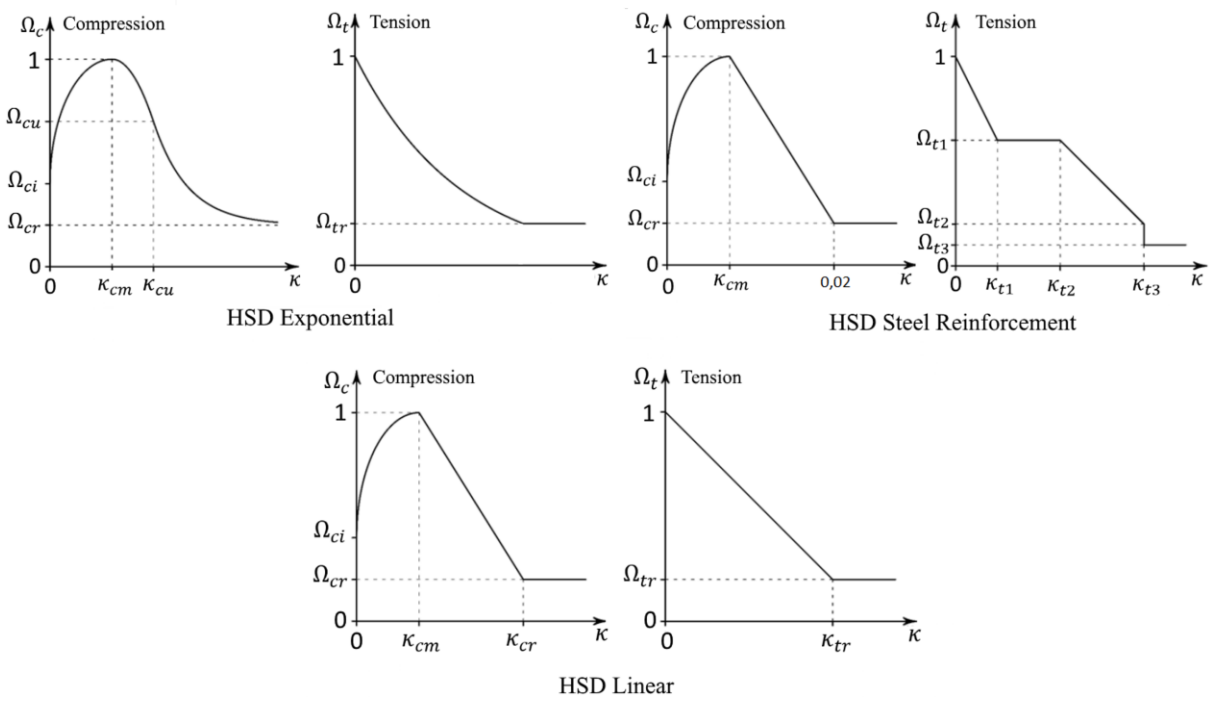

Figure 3. HSD Models (adapted from [6]).

In Fig. 3, the graphs represent the values of the softening and hardening functions in compression and tension (Ω_c and Ω_t) in the ordinates, and the effective plastic strain (κ) in the abscissa. The other parameters indicated in the graphs are input parameters, which can be adjusted to change the format of the functions, i.e., the constitutive laws are partially customizable. The softening laws in tension allow the effect of the contribution of concrete between cracks (known as tension stiffening phenomenon) to be considered.

2.2.2 Customized model via usermat

It was also used, for purposes of results comparison, a customized model for concrete developed by Lazzari et al. [7], based on the Ottosen criterion [4], through the ANSYS subroutine called usermat, which can be programmed to customize a material model [6], [10]. The surface of Ottosen [4] is given by Eq. (9) and (10).

$$f(I_1, J_2, \cos(3\theta)) = \alpha.\frac{J_2}{f_{cm}^2} + \lambda.\frac{\sqrt{J_2}}{f_{cm}} + \beta.\frac{I_1}{f_{cm}} - 1 = 0. \tag{9}$$

$$\lambda = \begin{cases} c_1.\cos\left(\frac{1}{3}arccos(c_2.cos(3\theta))\right) & for \;\; cos(3\theta) \geq 0. \\ c_1.\cos\left(\frac{\pi}{3} - \frac{1}{3}arccos(-c_2.cos(3\theta))\right) & for \;\; cos(3\theta) \leq 0. \end{cases} \tag{10}$$

Where f_{cm} is the average compressive strength of concrete; $\alpha, \beta, c_1 \; and \; c_2$ are material parameters.

For the compressive behavior, the hardening law adopted is given by Eq. (11), illustrated in Fig. 4(a), suggested by *fib2010* model code [11].

$$\frac{\sigma_c}{f_{cm}} = -\left(\frac{k.\eta - \eta^2}{1 + (k-2).\eta}\right). \tag{11}$$

Where σ_c is the compressive stress; ε_c is the compressive strain of concrete; ε_{c1} is the strain at the ultimate compressive stress; $\varepsilon_{c,lim}$ is the ultimate compressive strain; E_{ci} is the initial tangent modulus of elasticity of concrete; E_{c1} is the secant modulus of elasticity of concrete; $k = E_{ci}/E_{c1}$ is the plastic number; and $\eta = \varepsilon_c/\varepsilon_{c1}$.

For the tensile behavior, a model of distributed cracks was adopted, considering the tension stiffening effect through the softening law shown in Fig. 4 (b). Initially, the concrete is admitted as linear elastic until the tensile strength (f_{ctm}) is reached. After the cracking occurs, the softening is governed by a decreasing line that intersects the vertical axis in the value of $\alpha.f_{ctm}$ and the horizontal axis in the limit strain value (ε_{ctu}). In the present work, α=0.6 e ε_{ctu}=0.001 were adopted.

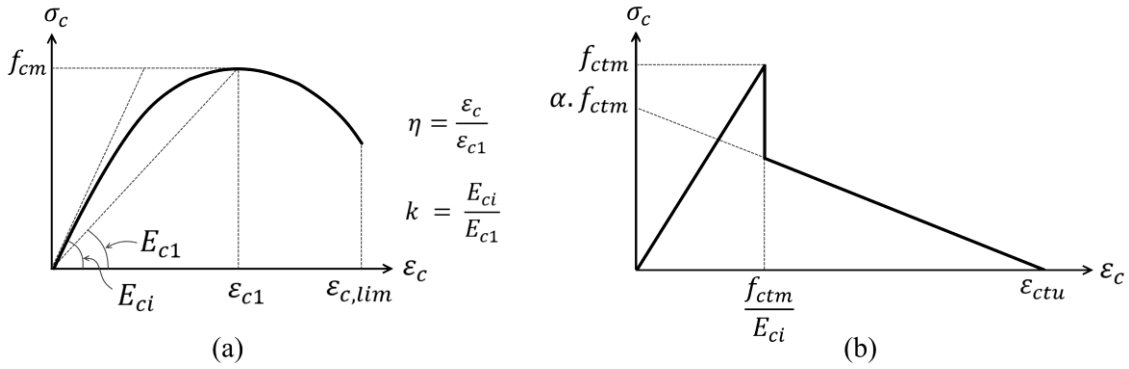

Figure 4. Constitutive laws for concrete in usermat model: (a) compression; (b) tension.

2.2.3 Steel models

The longitudinal reinforcement bars steel was modeled by von Mises plastification criterion for yielding with isotropic hardening. As hardening law, the constitutive model proposed by Gattesco [12], shown in Fig. 5 (a), was adopted. This model is divided into three stages of loading: (i) elastic-linear; (ii) yield plateau; (iii) hardening governed by parabolic curve, according to Eq. (12).

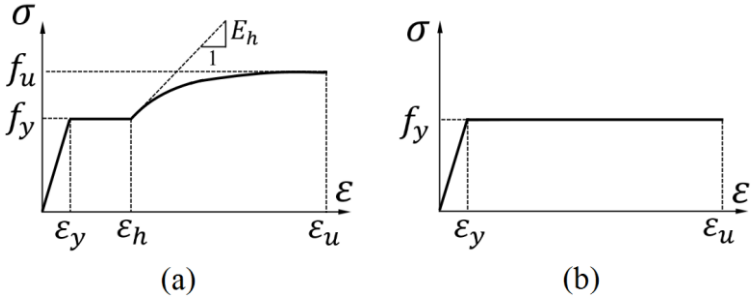

Figure 5. Constitutive laws for steel reinforcement: (a) longitudinal bars; (b) stirrups.

$$\sigma = f_y + E_h.(\varepsilon - \varepsilon_h).\left(1 - \frac{E_h.(\varepsilon - \varepsilon_h)}{4.(f_u - f_y)}\right). \tag{12}$$

Where f_y and f_u are the steel yielding and ultimate strengths, ε_y is the strain at steel yielding stress, ε_h is the strain at the initial hardening, ε_u is the strain at ultimate stress, E is the steel modulus of

elasticity and e E_h is the tangent modulus of elasticity.

On the other hand, stirrup steel was simplified as perfectly elastoplastic, as shown in Fig. 5 (b).

2.3 Boundary Conditions

The developed model admits the beams as simply supported and uses the symmetry condition. Thus, the nodes at the first support, on the lower face of the beam, had the displacements in y and z restricted; and the nodes at the central cross-section of the beam had the displacements in x and the rotations around y and restricted, as shown in Fig. 6. The total load is divided by two, due to the symmetry, and applied in the center of the span.

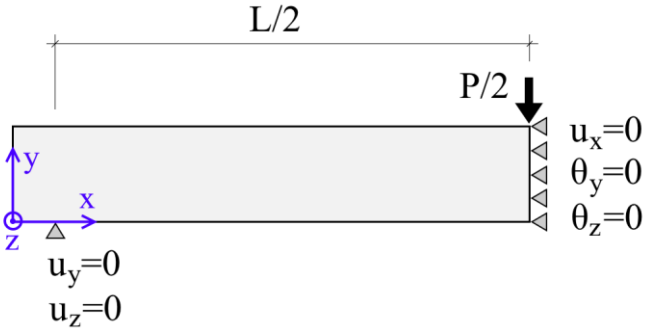

Figure 6. Boundary conditions.

3 Examples analyzed

Two beams, experimentally tested by Bresler and Scordelis [8], named A1 and A3, were modeled. The DP-Concrete analyses were performed with the three HSD models previously described and with the two available surface combinations – DP-DP and DP-Rankine – in order to compare the results between them. In addition, analyses were performed with the usermat model, and the results were also compared with those obtained by Lazzari [13], who simulated numerically these beams.

Figure 7 shows the geometry of the beams cross sections, the reinforcement arrangements and the data of the steel used, which were inserted in the numerical model. Figure 8 shows schematically the tests, which consisted in the application of concentrated loads on the midspan.

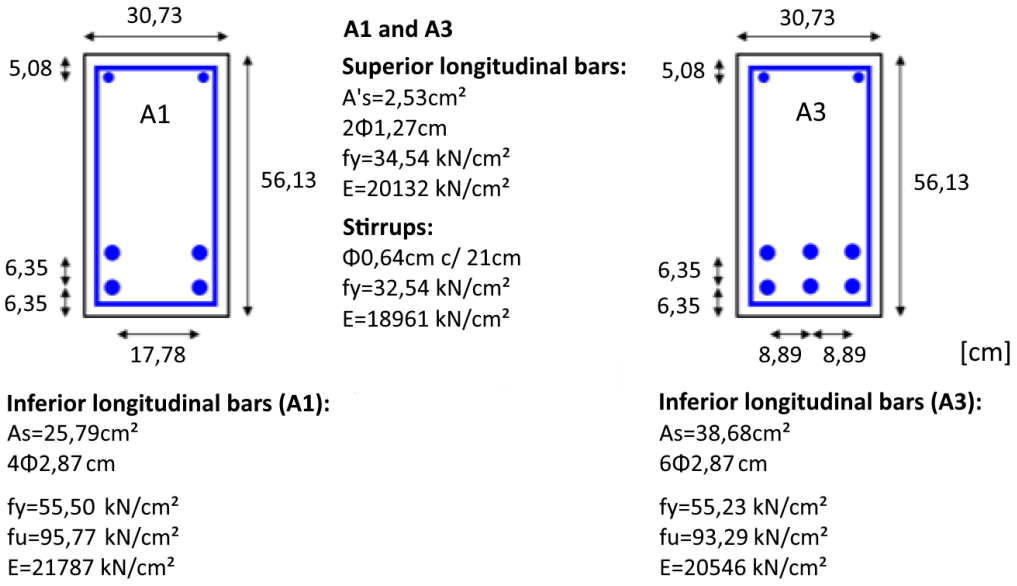

Figure 7. Cross sections of the beams A1 and A3 (adapted from [8] and [13]).

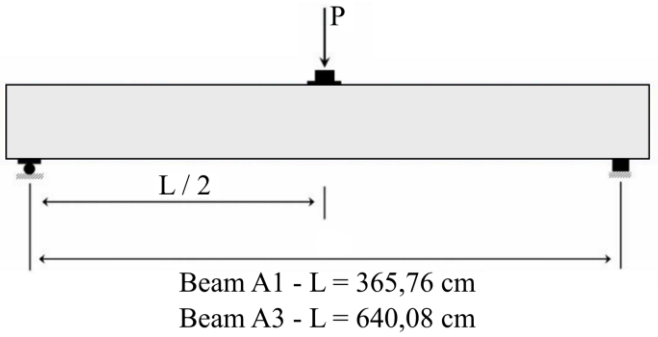

Figure 8. Schematic drawing of testing setup (adapted from [8] and [13]).

In addition to the data of Fig. 7, the values of $\varepsilon_h/\varepsilon_y$=1.5 and E_h=1000 kN/cm², were used for the numerical steel modeling of the inferior longitudinal bars with the constitutive model of Gattesco [12], adjusted to the results of tensile tests performed and made available by Bresler and Scordelis [8].

Table 1 shows the data used for the concrete, and indicates which values were provided by Bresler and Scordelis [8], obtained from the tests performed by the authors; and which were calculated by analytical expressions, such as the initial modulus of elasticity (E_{ci}), that was calculated according to the model code fib2010 [11]. For the analysis with the usermat, this initial modulus of elasticity was used; and for the analysis with the DP-Concrete a reduced modulus was used, since the initial domain of the stress-strain curve is approximated by a linear function until the stress reaches the value of $0.4.f_{cm}$. For this purpose, the value of $0.9.E_{ci}$ was adopted in the two analyzed beams.

The average tensile strength is calculated internally by the usermat model, automatically, as a function of f_{ck}, from an equation provided by the fib2010 code [11]. On the other hand, for the DP-Concrete model it is possible to provide the value of this resistance. In this case, since Bresler and Scordelis [8] provided the value of the tensile strength in bending ($f_{ct,f}$) obtained in a test, 70% of this value was used as the average tensile strength, as recommended by NBR 6118 [14]. For this reason, the values used for the tensile strengths in the DP-Concrete model were slightly different from the values used in the usermat and Lazzari [13] models.

Table 1. Concrete parameters used in numerical models.

Parameter	Beam		Unit	Equation/Source	Numerical parameter	
	A1	A3			DP	Usermat
f_{cm}	2.41	3.50	kN/cm²	Bresler and Scordelis[8]	R_c	f_{cm}
$f_{ct,f}$	0.39	0.43	kN/cm²	Bresler and Scordelis[8]	-	-
f_{ctm}	0.27	0.30	kN/cm²	$0.7.f_{ct,f}$[14]	R_t or T	-
f_{ck}	1.61	2.70	kN/cm²	$f_{cm} - 0.8$ [11]	-	f_{ck}
f_{ctm}	0.19	0.27	kN/cm²	$0.03.(10.f_{ck})^{2/3}$[11]	-	f_{ctm}
f_{c2m}	2.83	4.08	kN/cm²	$f_{cm}.(1.2 - f_{cm}/100)$ [11]	R_b	f_{c2m}
E_{ci}	2883	3264	kN/cm²	$2150.(f_{cm})^{1/3}$ [11]	-	E_{ci}
E_c	2595	2938	kN/cm²	$0.9.E_{ci}$	E_c	-

The parameters used for the HSD models (see Fig. 3) are presented in Table 2. In order to calculate the values of the effective plastic strains at the points considered, the elastic strains were discounted from the total strains. The total strain at the maximum stress point was assumed to be 2.1‰, and the ultimate total strain was assumed to be 3.5‰. Figure 9 shows the numerical models of the beams A1 and A3.

Table 2. Parameters used in HSD models.

Linear		Exponential		Steel Reinforcement	
κ_{cm}	$0.0021 - R_c/E_c$	κ_{cm}	$0.0021 - R_c/E_c$	κ_{cm}	$0.0021 - R_c/E_c$
κ_{cr}	$0.0035 - \Omega_{cr}.R_c/E_c$	κ_{cu}	$0.0035 - \Omega_{cu}.R_c/E_c$	Ω_{ci}	40%
Ω_{ci}	40%	Ω_{ci}	40%	Ω_{cr}	10%
Ω_{cr}	65%	Ω_{cu}	65%	κ_{t1}	0.0001
κ_{tr}	0.001	Ω_{cr}	40%	κ_{t2}	0.00011
Ω_{tr}	2%	Ω_{tr}	2%	κ_{t3}	0.001
-	-	-	-	Ω_{t1}	60%
-	-	-	-	Ω_{t2}	2.1%
-	-	-	-	Ω_{t3}	2%

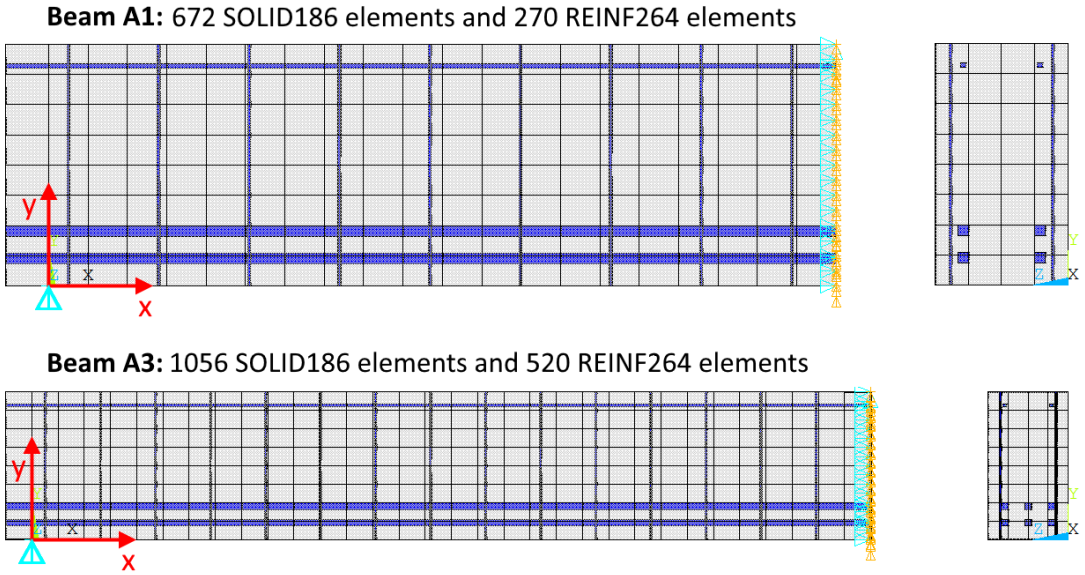

Figure 9. Finite element models for beams A1 and A3.

It should be noted that the HSD Exponential model has an extra input parameter for the tensile behavior, besides those shown in Table 2, which is the specific fracture energy per area (G_{ft}), in kN.cm/cm². From some tests performed on simpler models, it was verified that this parameter is dependent on the elements size. Through the algebraic manipulation of equations provided by the software manual [6], Eq. (13) was deduced.

$$G_{ft} = -\frac{\bar{\kappa}.R_t.L_i}{\ln(\Omega_{tr})}. \tag{13}$$

Where $\bar{\kappa}$ is the effective plastic strain when the HSD function in tension reaches the residual stress (see Fig. 3); $L_i = \sqrt[3]{V/8}$, and V is the element volume. In this work $\bar{\kappa}$=0,0018 was assumed, and, from this value, $G_{ft}$was calculated with Eq. (13), considering the elements volumes of each beam analyzed.

4 Results and discussion

Figures 10 and 11 present the obtained results by the present work, with the different models used, of the total load applied versus midspan deflection relationships for the beams A1 and A3, along the experimental results by Bresler and Scordelis [8] and numerical results by Lazzari [13].

In the experimental test, the beam A1 presented shear compression failure, with crushing of the compressed diagonals due to shear. However, the beam A3, with a significantly larger span, failed by crushing of the compressed zone in the midspan, due to bending [8].

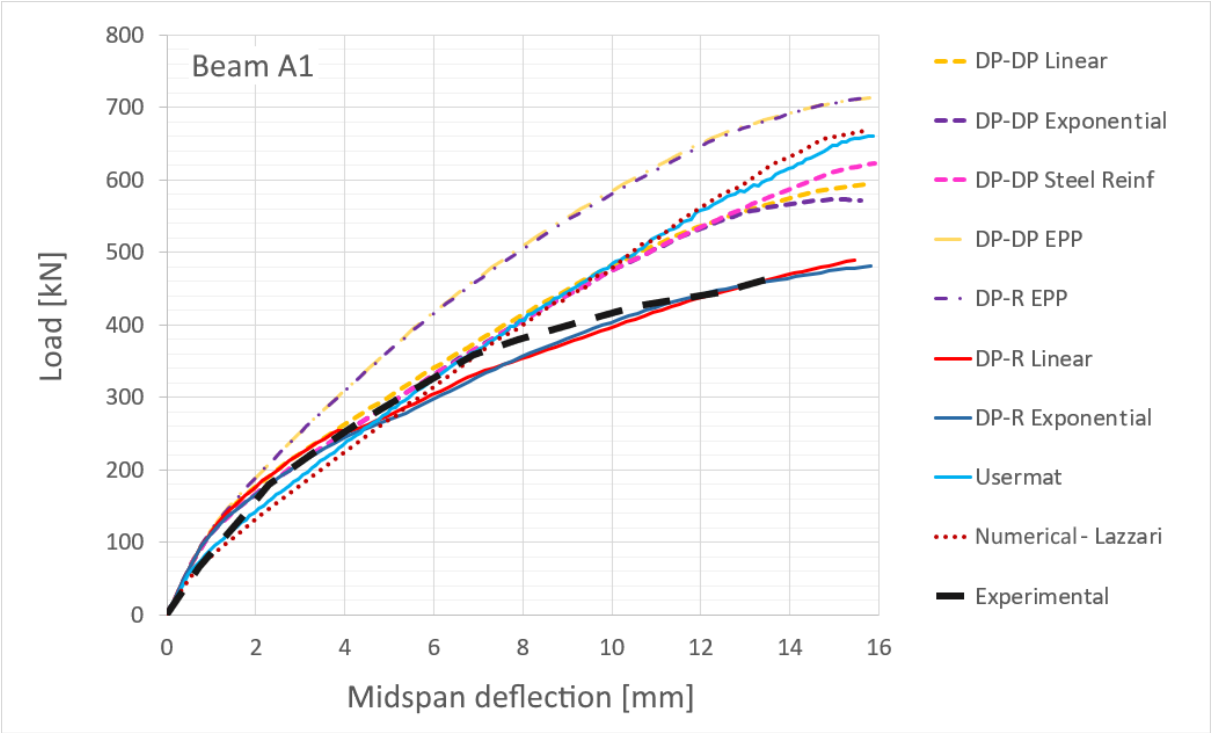

Figure 10. Load-deflection curve – Beam A1.

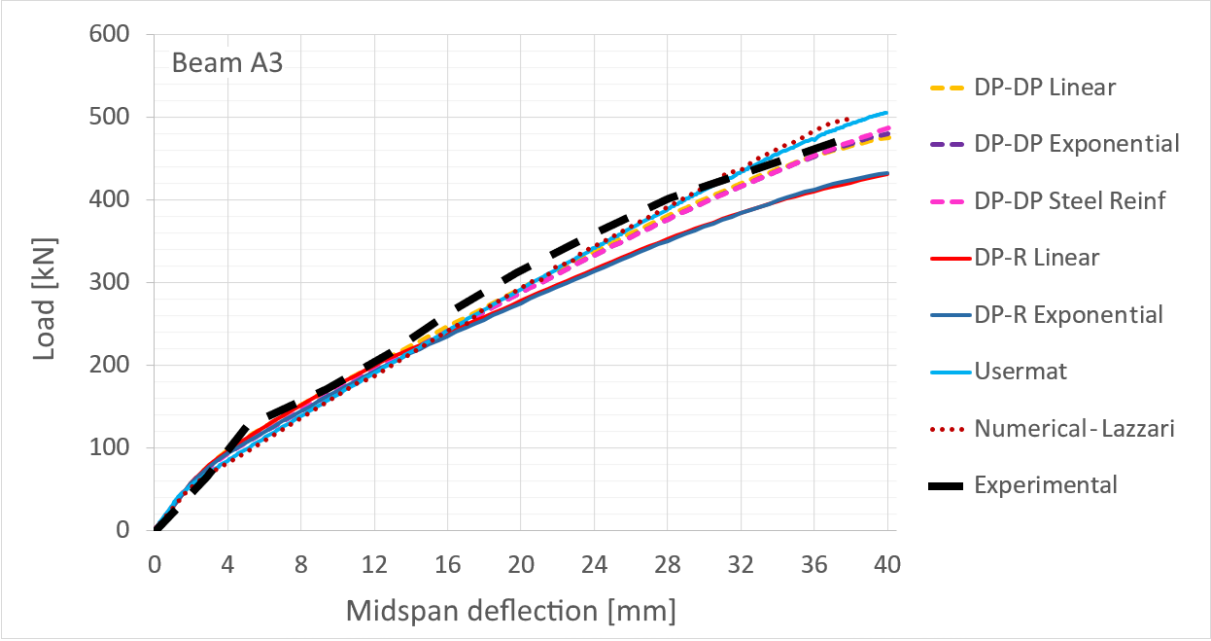

Figure 11. Load-deflection curve – Beam A3.

It is observed that the models with the combination of surfaces DP-Rankine that used Linear and Exponential HSD models obtained very good results for beam A1. For beam A3, these two models captured well the response at the initial loading, as well as the beginning of the cracking phenomenon

and the transition to stage 2, but presented differences slightly larger than the other models in the final stage of loading, although relatively small. In general, however, analyzing the two graphs, it is possible to affirm that, among the DP-Concrete models available, these two options presented the best results for the analyzed beams. It should be noted that the HSD Linear model has the advantage that its input data are mesh independent, unlike the HSD Exponential model, that uses the mesh dependent area-specific fracture energy (G_{ft}). The HSD Steel Reinforcement model cannot be applied to the DP-Rankine combination, being restricted to the DP-DP combination [6].

The three models with the combination of surfaces DP-DP, which used the Linear, Exponential and Steel-Reinforcement HSD models, presented very similar results to each other. They simulated very well the behavior of beam A3 throughout the analyzed domain but failed to capture the final stage of loading of beam A1, when the compressed diagonals crushed in the experimental test.

The numerical model of the present study that used the usermat presented results close to those of the DP-Concrete models with DP-DP combination, and practically reproduced the numerical results obtained by Lazzari [13], who also used the same usermat. The subtle differences that are observed occur in function of the different meshes adopted and the constitutive model for the steel of the longitudinal reinforcement bars.

The perfect elastoplastic models (EPP), as expected, overestimated the strength of beam A1, since they do not use softening rules in tension and compression, and therefore do not adequately simulate cracking and crushing. In any case, these models are interesting within the logic of gradual refinement of the results, since they serve as superior limiters for the beam response and can be very useful in preliminary tests and analyses.

Cracking: In the DP-Concrete model, cracking is simulated in a simplified way by plastic strains, which are related to a softening rule in tension. Therefore, one way of verifying the evolution of cracking in concrete is to visualize the plastic strains of the model. Figure 12 shows the equivalent plastic strains of the beam A3, at the ultimate load, obtained by the DP-Rankine model with HSD Exponential, and the last experimental cracking pattern observed experimentally, as presented by Bresler and Scordelis [8]. It is verified that the numerical model is able to capture the cracking state in a global way, correctly indicating the regions in which this phenomenon occurs, although it is not able to capture localized effects with great precision, which was already expected, since works within the logic of distributed cracking models.

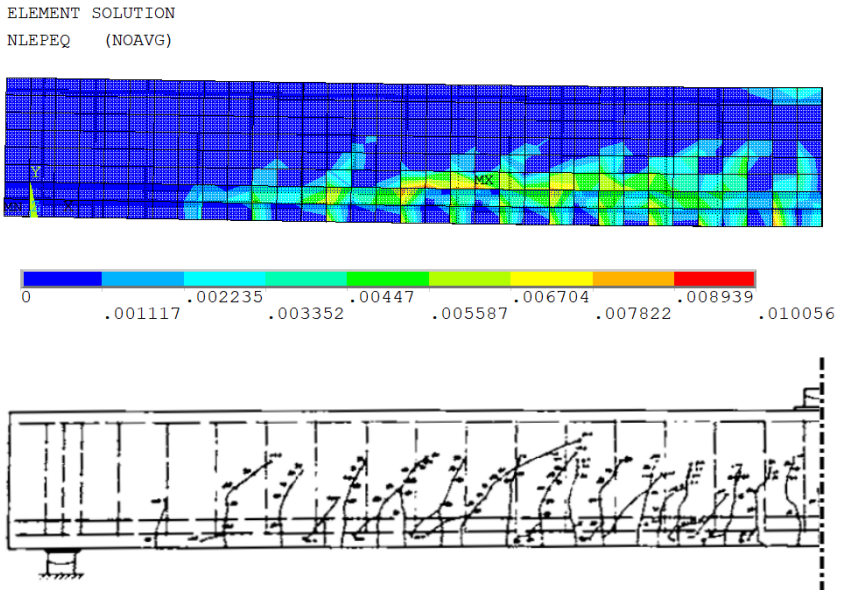

Figure 12. Beam A3 experimental cracking pattern [8], and plastic strains from numerical simulation.

5 Conclusions

A finite element numerical model was developed in ANSYS software, version 19.2, for the simulation of reinforced concrete beams, using a new material model, called DP-Concrete, made available by the software in its most recent versions and consisting of a combination of two plastification surfaces: one for tension (Drucker-Prager or Rankine) and one for compression (Drucker-Prager). The obtained results with this model showed good correlation with the experimental results of two beams tested by Bresler and Scordelis [8]. The two possibilities of surface combinations (DP-DP or DP-Rankine) and three HSD models provided by the software were used. There were differences between the results obtained with the two combinations, especially in the analysis of beam A1, for which the model with the DP-Rankine combination presented better results in the vicinity of the ultimate load.

Analyses were also performed with a customized material model, based on the surface of Ottosen [4], and its results were similar to those obtained with the DP-Concrete model, especially with the DP-DP combination.

Finally, it is concluded that the DP-Concrete model was able to properly simulate the two analyzed beams, and has great potential for use, since it employs two very simple surfaces (Rankine and Drucker-Prager) in its formulation, which facilitates the convergence process of the non-linear solution. In addition, the model proved to be quite versatile and flexible, as it offers two options of surface combinations and different HSD models with adjustable parameters. In this way, it is possible to work within the logic of gradual refinement of results, gradually incorporating nonlinearities into the model, comparing results and developing a more reliable numerical model.

Acknowledgements

The authors are grateful to CAPES and CNPq for their financial support for this research activity, and to CEMACOM/UFRGS for the infrastructure to carry out this work.

References

[1] W. F. Chen. *Plasticity in reinforced concrete*. McGraw-Hill, 1982.
[2] D. C. Drucker and W. Prager. Soil mechanics and plastic analysis or limit design. *Journal of Applied Mathematics*, v. 10, n. 2, pp. 157–165, 1952.
[3] K. J. Willam and E. P. Warnke, 1975.Constitutive model for the triaxial behavior of concrete. In: IABSE Proceedings, *IABSE Seminar on Concrete Structures Subjected to Triaxial Stresses*, pp. 1–30.
[4] N. S. A. Ottosen. Failure criterion for concrete. *Journal of the Engineering Mechanics Division ASCE*, v. 103, pp. 527–535, 1977.
[5] F. D. Queiroz, P. C. G. S. Vellasco and D. A. Nethercot. Finite element modelling of composite beams with full and partial shear connection. *Journal of Constructional Steel Research*, v. 63, n. 4, pp. 505–521, 2007.
[6] ANSYS Inc. ANSYS help system: version 19.2. Canonsburg, 2018.
[7] P. M. Lazzari, A. Campos Filho, B. M. Lazzari, A. R. Pacheco and R. R. S. Gomes. Numerical simulation of the constructive steps of a cable-stayed bridge using ANSYS. *Structural Engineering and Mechanics*, v. 69, n. 3, pp. 269–281, 2019.
[8] B. Bresler and A. C. Scordelis. Shear Strength of Reinforced Concrete Beams. *Journal of the American Concrete Institute*, v. 60, n. 1, pp. 51–74, 1963.
[9] O. C. Zienkiewicz. *The Finite Element Method*. McGraw-Hill Company, 1977.
[10] F. P. Quevedo, R. J. Schmitz, I. B. Morsch, A. Campos Filho and D. Bernaud. Customization of a software of finite elements to analysis of concrete structures: long-term effects. *Revista Ibracon de Estruturas e Materiais*, v. 11, n. 4, pp. 696–718, 2018.
[11] Féderation Internationale du Béton. *Model code fib2010*. Bulletin n. 65. Lausanne, 2012.
[12] N. Gattesco. Analytical modeling of nonlinear behavior of composite beams with deformable connection. *Journal of Constructional Steel Research*, v. 52, pp. 192–218, 1999.

[13] P. M. Lazzari. Simulação numérica das etapas construtivas de pontes estaiadas através do método dos elementos finitos. PhD thesis, Universidade Federal do Rio Grande do Sul, 2016.
[14] Associação Brasileira de Normas Técnicas. *NBR 6118*: projeto de estruturas de concreto – procedimento. Rio de Janeiro, 2014.